crystals

MDPI

Article

Fracture Behavior of Single-Crystal Sapphire in Different Crystal Orientations

Shizhan Huang [1,2], Jiaming Lin [1,2], Ningchang Wang [3,4], Bicheng Guo [1,2], Feng Jiang [1,2,*], Qiuling Wen [1,2] and Xizhao Lu [5]

1 Institute of Manufacturing Engineering, Huaqiao University, Xiamen 361021, China; 1611411015@stu.hqu.edu.cn (S.H.); linjiaming@hqu.edu.cn (J.L.); Guobicheng1@stu.hqu.edu.cn (B.G.); qlwen@hqu.edu.cn (Q.W.)
2 National & Local Joint Engineering Research Center for Intelligent Manufacturing Technology of Brittle Materials Products, Xiamen 361021, China
3 Zhengzhou Research Institute for Abrasives & Grinding Co., Ltd., Zhengzhou 450001, China; wangningchang@126.com
4 State Key Laboratory of Superabrasives, Zhengzhou 450001, China
5 College of Mechanical Engineering and Automation, Huaqiao University, Quanzhou 361021, China; luxizhao@hqu.edu.cn
* Correspondence: jiangfeng@hqu.edu.cn

Abstract: In order to study the anisotropy of fracture toughness and fracture mechanism of single-crystal sapphire, the three-point bending tests and the single-edge V-notch beam (SEVNB) were used to test the fracture toughness of A-plane, C-plane, and M-plane sapphire, which are widely used in the semiconductor, aerospace, and other high-tech fields. Fracture morphology was investigated by a scanning electron microscope and three-dimensional video microscopy. The fracture toughness and fracture morphology of different crystal planes of sapphire showed obvious anisotropy and were related to the loading surfaces. C-plane sapphire showed the maximal fracture toughness of 4.24 MPa·m$^{1/2}$, and fracture toughness decreases in the order of C-plane, M-plane, and A-plane. The surface roughness is related to the dissipation of fracture energy. The surface roughness of the fracture surface is in the same order as C-plane > M-plane > A-plane. The fracture behavior and morphology of experiments were consistent with the theoretical analysis. C-plane sapphire cleavages along the R-plane with an angle of 57.6 degrees and the rhombohedral twin were activated. M-plane and A-plane sapphire cleavages along their cross-section.

Keywords: single crystal sapphire; fracture toughness; three-point bending test; single-edge V-notch beam; cleavage

Citation: Huang, S.; Lin, J.; Wang, N.; Guo, B.; Jiang, F.; Wen, Q.; Lu, X. Fracture Behavior of Single-Crystal Sapphire in Different Crystal Orientations. *Crystals* **2021**, *11*, 930. https://doi.org/10.3390/cryst11080930

Academic Editor: Tomasz Sadowski

Received: 19 June 2021
Accepted: 6 August 2021
Published: 11 August 2021

1. Introduction

Due to their ultra-high hardness, wear resistance, corrosion resistance, and excellent light transmittance, sapphire materials are widely used in the aerospace industry, national defense [1], optical industry, substrate manufacturing, etc. [2]. However, it is difficult to process the precision sapphire parts with complex structures or high surface quality, due to the high brittleness of sapphire materials. As one of the intrinsic mechanical properties of sapphire materials, fracture toughness is the only indicator of characterization materials to resist crack extension and material brittleness. The fracture toughness of brittle material (single crystal, glass, polycrystalline ceramic) can greatly affect the removal processing of the material and subsurface damage. Optimizing the processing of brittle materials, it was essential to control fracture (crack propagation) to reduce the depth of harmful surface damage [3]. Single crystal sapphires with different crystal plane orientations have different uses in the industry. In this paper, the fracture toughness and mechanism of different crystal plane orientations were studied, which can be used as the basis for industrial material selection and machining to avoid the great harm caused by brittle fracture at low stress.

There are many ways to test the fracture toughness of brittle materials. Prefabricating the initial cracks of the appropriate length, can be used to accurately evaluate the fracture toughness of the material [4–6]. Zhao et al. used a femtosecond laser to prefabricate super sharp V-notch in the single-edge V-notch beam (SEVNB) method to obtain the fracture toughness of structural ceramics accurately and reliably [7]. Quinn et al. used the surface crack in flexure (SCF) method and the single-edged pre-cracked beam (SEPB) method to test the fracture toughness of glass. The accuracy of the test results was largely determined by the quality of the prefabricated cracks [8]. Yanaba et al. discussed the relationship between fracture toughness and flexural fracture area of WC-10 mass% Co cemented carbide and silicon nitride ceramics. The experimental results of the SEPB method were in good agreement with the results of theoretical calculation [9].

However, many researchers focus on the fracture mechanism of anisotropic materials, such as ceramics, glass, and cemented carbide. Due to anisotropy, the physical, chemical, and optical properties of materials with different crystal orientations show obvious differences, which have a great impact on the processing performance of materials, and seriously affect the material removal and the surface quality of processing. The optimal machining direction can be obtained by defining the fracture behavior of these materials. In the ultra-precision machining of KDP crystal, Zhao et al. found that the change of cutting force was caused by the anisotropy of crystal, and the change of roughness was also related to the anisotropy [10].

Due to the characteristic hexagonal crystal structure and obvious anisotropy material of single-crystal sapphire, the processing of sapphire is challenging. Studying the fracture and removal mechanisms of sapphire is very essential for the optimization of processing parameters.

In order to study the material removal rate (MRR) and workability of sapphire with different crystal orientations, Wen et al. performed focused ion beam (FIB) milling on single-crystal sapphire with A-, C-, and M-orientations. The experimental results show that: The MRR of A-plane sapphire is slightly higher than that of C-plane and M-plane sapphires; and the *S*a of A-plane sapphire, after FIB treatment, is the smallest among the three different crystal orientations [11]. In addition, Wen et al. irradiated sapphire with different crystal orientations by the femtosecond laser, and the damage threshold of C-plane < M-plane < A-plane < R-plane was obtained. The damage accumulation of sapphire with M-plane was the largest, and it was easier to form cracks under multi-pulse irradiation [12]. Wang et al. revealed the removal mechanism for each orientation of single-crystal sapphire by double-sided planetary grinding experiments. The R-plane was removed in the form of large pieces of spalled material and had the highest MRR and the largest surface roughness (*S*a) of approximately 780 nm among the orientations studied. The C-plane was mainly removed in the form of unique large step-like pieces of spalled material, had the lowest MRR among the orientations observed, and exhibited an *S*a of approximately 430 nm [13]. Luo et al. used the sol-gel (SG) polishing pad to machine the C-plane, A-plane, and M-plane sapphires. The polishing results showed that the C-orientation, with a surface roughness of about 2 nm, is smoother than the A- and M-orientations and the MRR of C-orientation is higher than that of them [14]. Wang et al. used a diamond wire saw to cut A-plane sapphire in different cutting directions to explore its machinability. It was concluded that the cutting direction along the M-plane was the best, considering the minimum cutting force and the minimum material volume removal could be obtained [15].

To study the mechanism of crack propagation and fracture damage evolution of sapphire with different crystal orientations, Luan et al. performed dynamic and quasi-static indentation tests on the c-plane and a-plane of sapphires by Hopkinson pressure bar tester and continuous indentation tester, respectively. It was found that the bearing capacity of sapphire is related to the loading velocity, while the crack propagation is affected by the crystal orientation. The R-planes of sapphire are weaker than other crystal planes and are prone to crack propagation [16]. Jiang et al. tested the dynamic mechanical properties of C-plane sapphire by also using the Hopkinson pressure bar tester. The true stress-strain curve

of sapphire has been obtained at different velocities. It was found that the crystal orientation influences the crack path and crack pattern, which leads to different energy consumption during crack propagation [17]. Wang et al. used a Vickers indenter on a micrometer scale to study crack propagation that is induced by sequential indentation was investigated on the A-plane and C-plane of sapphire. Due to the different slip systems induced by an indentation on the different crystal planes of sapphire, increasing the indentation depth obviously increases the rate of crack propagation on the A-plane, but this effect is not so obvious on the C-plane. Moreover, some parallel linear traces along the A-plane, which fracture with increasing indentation depth, are observed from the residual indentation on the A-plane [18]. Wang et al. performed impact and static load tests on the A-plane, C-plane, M-plane, and R-plane of sapphire by the high-frequency cyclic impact test device, respectively. It was found that the crack propagation is affected by the crystal orientation, which leads to different characteristics of the surface morphology of the different crystal orientations sapphire after a fracture. Moreover, four different models of the crack system are proposed for A-plane, C-plane, M-plane, and R-plane, respectively [19]. Wan et al. found that the surface damage depth of the A-plane sapphire was greater than that of C-plane sapphire by precision grinding. The subsurface cracks of A-plane sapphire included transverse and radial cracks, while the subsurface cracks of C-plane sapphire were mainly transverse [20].

The occurrence of pop-in events at micro-scale always presents ductile-brittle transition. Wang et al. developed a mechanical model for pop-in events of sapphire based on indentation test results obtained by a Rockwell indenter with a tip radius of 4.5 μm. The predicted pop-in loads showed good agreement with experimental values for sapphires with different crystal orientations. The pop-in load for the C-plane sapphire was the largest, followed in the order of M-plane, A-plane, and R-plane sapphires under the same load conditions [21].

To study the relationship between plastic deformation and fracture of sapphire, Lin et al. used the molecular dynamics method to simulate the nanoindentation process of sapphire. The results showed that the activation of the twin/slip system has an important influence on the sapphire indentation morphology [22]. Besides, Lin et al. studied the influence of the scratching direction on surface morphology, stress distribution, and subsurface defects. The scratching surface morphology of sapphire is affected by the activation of slip systems. A smaller thickness of the subsurface damage layer was resulted by scratching along (1-010) and (1-100) directions [23].

The fracture mechanism and fracture toughness of single-crystal sapphire was studied by fracture mechanics experiments. Azhdari et al. prepared notched samples of sapphire with different crystal orientations. Through the compression fracture test, it was found that most of the samples fractured along the weak cleavage plane, and the two weakest families of cleavage planes were (-1012) and (10-11), especially, plane (-1102), plane (-1100) and plane (1-102) were the preferred fracture planes [24]. Konstantiniuk et al. used chemical vapor deposition to deposit single crystal and polycrystalline α-Al_2O_3 coatings on sapphire substrates with different crystal orientations, and prepared unnotched and notched microcantilevers. The (11-20) single crystalline coating which was aligned for fracture on the C-plane, exhibited the highest fracture stress and fracture toughness [25]. Graça et al. used the SEVNB method to explore the fracture resistance of single-crystal sapphire with different crystal orientations prepared by two processes. Estimation of the mosaic block boundary energy and application of the Griffith criterion for intergranular crack propagation allows the critical deflection angle below which intergranular fracture can take place to be determined [26].

Many researchers have tested the fracture toughness of sapphire with different crystal orientations, but there are still few reports on the relationship between the anisotropic fracture mechanism and fracture toughness of sapphire.

In this paper, the fracture toughness of single-crystal sapphire with different crystal orientations was tested by three-point bending tests. Single crystal sapphire samples were

prepared by the single-edge V-notch beam (SEVNB) method, including C-plane (0001), A-plane (11-20), and M-plane (10-10) sapphires. In addition, this paper further considered the influence of the loaded surface during the three-point bending tests. Microscopic morphology of the fracture surface was studied by a scanning electron microscope (SEM), three-dimensional video microscopy. In addition, the roughness of the fracture surface was tested by a three-dimensional optical profiler. To study the anisotropy of single-crystal sapphire with different crystal orientations, the result of fracture toughness, displacement-load curves, and fracture surface roughness were compared. The fracture mechanism was studied by the microscopic surface morphology of the fracture surface and the activation of the twin/slip system.

2. Design of Experiments

2.1. Sample Preparation and Orientation

Single-crystal sapphire is a simple coordination type oxide crystal, belonging to the hexagonal crystal system, with lattice parameters $a = b = 0.4758$ nm, $c = 1.2991$ nm, $\alpha = \beta = 90^\circ$, $\gamma = 120^\circ$. It is a typical anisotropic material, and Figure 1 shows the crystal structure of the single-crystal sapphire [1].

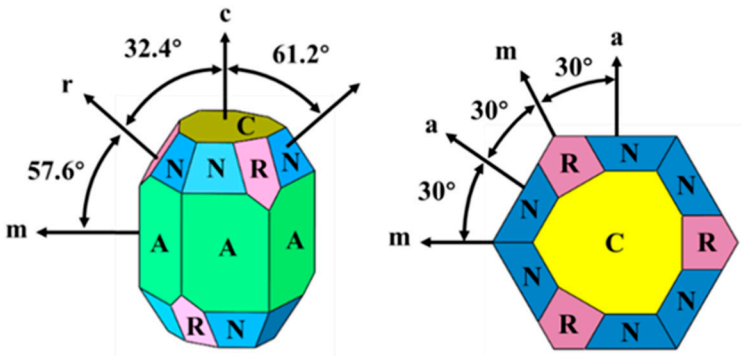

Figure 1. Crystal structure of the single-crystal sapphire.

Cleavage fracture is a kind of transgranular fracture under normal stress. The fracture surface is separated along a certain crystal plane (cleavage plane). Low temperature, impact load, and stress concentration often promote cleavage fracture. Sapphire has been considered completely uncleavable for a long time. In theory, it has nine cleavage surfaces. Six planes are parallel to the facets {11-20} and {10-10}, and to the C-axis; three planes are parallel to the facets {10-11}, the normal vectors to them make an angle of 57° with the C-axis. The cleavage in sapphire occurs at the intersection of a pair of parallel nets formed by anions. The larger the distance between the nets, the more vividly the cleavage manifests itself. In a perfect crystal, the plane of chipping must pass between these nets. In the basal plane with interchanging O-Al-Al-O-Al-O layers, there are no conditions for cleavage, whereas in the plane (10-11) with interchanging O-O-Al-O-Al-O-O-O-Al-O-Al-O layers the bonds between the layers O-O located at a distance of 1.06 Å are weakened. So, the crystals with a small number of dislocations and which do not contain blocks may have perfect cleavage in the plane of the morphological rhombohedron {10-11} [27].

Due to the sapphire plastic deformation scale is relatively small, material removal is multi-manifestation in actual processing. It is formed by the development of the brittle-ductile transition of sapphire. The plastic deformation of sapphire is mainly twin and slip, as shown in Table 1, which was summarized by Nowak et al. at room temperature [28]. The critical resolved shear stress (CRSS) of rhombohedral twin and basal twin is the smallest, and far less than other twin and slip systems. The second is cylinder slip and rhombic slip. Due to the CRSS required for base plane slip is the largest, it is more difficult to occur than other twin and slip systems. Two major twins are the foundation (C-plane) twins and rhombohedronal plane (R-plane) twins. Twinning in the planes {1011} is characterized by a lesser specific shear and is observed even at cryogenic temperatures.

Table 1. The twin and slip systems of sapphire at room temperature [28].

Number	Twin & Slip Systems	Plastic Deformation Type	Critical Resolved Shear Stress (GPa)
1	<01-11> {01-12}	Rhombohedral twin (RT)	0.111
2	<1-100> {0001}	Basal twin (BT)	0.148
3	<2-1-10> {01-12}	Rhombohedral slip (RS)	3
4	<2-1-10> {0001}	Basal slip (BS)	17
5	<1-210> {10-10}	Prismatic slip (PRS)	1.2

In this paper, three sapphire samples with different crystal orientations were produced by Jiangsu Ruibo Optoelectronics Technology Co., Ltd. The raw materials were cut into 35 mm × 3 mm × 4 mm rectangular bars, and then polished by CMP to reach the surface roughness Ra lower than 0.3 nm, as shown in Figure 2.

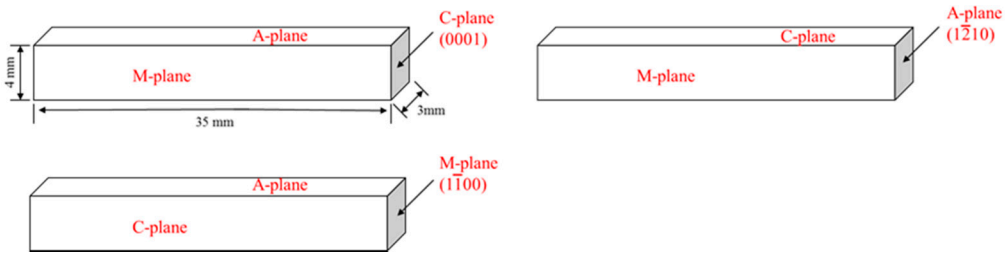

Figure 2. Three different crystal orientations of sapphire samples.

2.2. Three-Point Bending Test and SEVNB

There are several testing methods for fracture toughness. The single edge notched bend bar (SENB) method is simple to prepare samples, and the test system is easy to operate. However, the width of the incision is limited by the thickness of the diamond blade, and a passivation effect will occur at the root of the incision, causing the measured fracture toughness to be higher than the true value [29]. The single edge pre-cracked beam (SEPB) method, also known as the bridge compression method, is the most reliable and accurate test method [30]. The test results of the indentation method (IM) are related to the smoothness of sample surface, crack form, and calculation formula, and the results under different conditions have large deviation [31]. The single-edge V-notch beam (SEVNB) method was adopted in this work, due to its good repeatability [32].

In this study, the three-point bending test and SEVNB method were based on ISO 23146 [33]. The three-point bending tests were performed by the universal testing machine typed Sans 5305, and the sample fixture was shown in Figure 3a. The sample was placed horizontally on the two bearing rollers. The height of the two bearing rollers was consistent. The two bearing rollers were parallel and perpendicular to the length direction of the sample. Their spacing is 30mm. The radius of the pressure head and bearing rollers is 1.6 mm. The symmetrical center line intersected the centerline of the main shaft of the universal testing machine vertically.

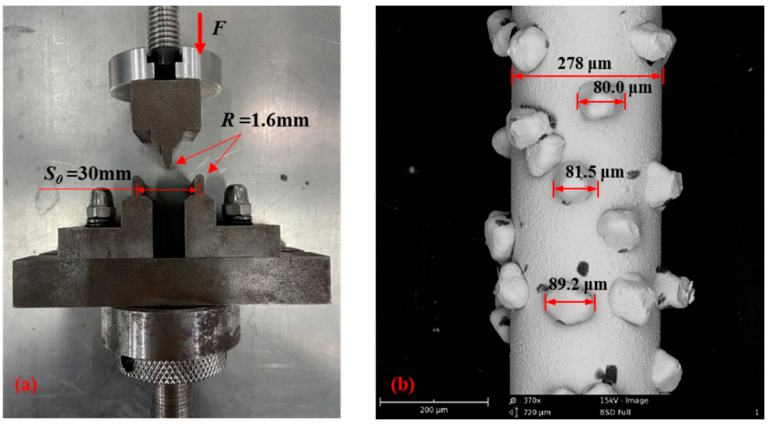

Figure 3. (**a**) Sample fixture for the three-point bending test, where F is the loading force, R is the radius of pressure head and bearing rollers, and S_0 is the span of three-point bending. (**b**) Diamond wire saw.

A sudden pre-crack in the middle of the sample was prepared by two steps. In the first step, the U-notch groove was processed by a diamond wire saw in the middle of the loading plane. The wire diameter of diamond wire saw is 280 μm, the diameter of diamond particles is 80–90 μm, as shown in Figure 3b. In the second step, the V-notch was processed by a laser at the bottom of the U-notch groove. The details of processing parameters were shown in Table 2. The cutting depth was 2 mm. Due to the wire diameter, the actual cutting depth was about 1 mm. The cutting depth of the laser was about 0.5 mm.

Table 2. Preparing the standard sample.

Steps	Machine	Parameter	Result
Step 1: Preparing the U-notch groove	Diamond wire cutting machine of Shenyang kejing STX-402	V_c = 1.8 m/s V_f = 0.3 mm/min ap = 2 mm	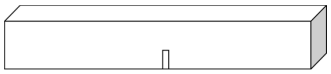
Step 2: Preparing the V-notch	Laser machine of SCABNLAB BasiCube10 SN:545393	λ= 355 nm τ = 15 ns V_s = 1 mm/s f = 50 kHz d = 10 μm n = 10	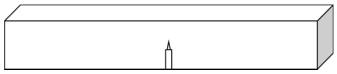

Where V_c is the linear velocity of diamond wire, V_f is the feed rate of diamond wire, ap is the cutting depth, W is the pulse width of laser, V_s is the scanning speed, f is the laser frequency, d is the spot diameter of laser, and n is the repetition times of laser scanning.

Single-crystal sapphire samples with different crystal orientations have one cross-section and two side-faces. In addition to the cross-section, different side-faces in its length will be loaded separately in this study. Therefore, the test groups were named as "Number-Cross-section-Loaded surface", with a total of six test groups, as shown in Table 3. For example, the test "1-M-A" is the first test group, "M" is the cross-section of the sapphire sample, and "A" is the loaded surface of the sapphire sample. Each group prepared 7 samples and repeated the independent test seven times.

Table 3. Testing groups.

Test Groups	Cross-Section	Loaded Surface	Test Groups	Cross-Section	Loaded Surface
1	M	A	4	C	A
2	M	C	5	A	C
3	C	M	6	A	M

Where M is the crystal orientation of (10-10), C is the crystal orientation of (0001), and A is the crystal orientation of (11-20).

This test was in the air and at room temperature. The pressure head of the testing machine was set to a load at a constant rate of V = 0.05 mm/min, and the direction was vertical down. The loading time, loading force, and displacement were recorded.

After the samples are fractured, according to ISO 23146 [33], the ideal fracture morphology is shown in Figure 4, where part 1 is the fracture surface, part 2 is the processing surface of the pre-fabricated crack. On the fracture surface, the V-notch depths at $B/4$, $B/2$, and $3B/4$ along the width of the sample were selected for measurement and denoted as a_1, a_2, a_3.

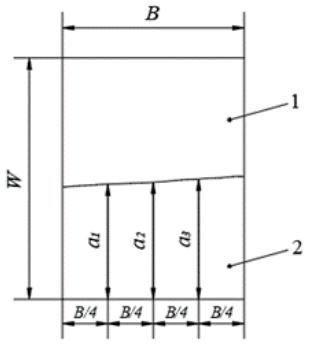

Figure 4. Ideal fracture surface.

The average depth of the V-notch is calculated using Formula (1), denoted as a, and must satisfy the Formula (2) to lower the calculation error. The average relative V-notch depth is calculated using Formula (3) and denoted as α.

$$a = (a_1 + a_2 + a_3)/\ 3 \tag{1}$$

$$(a_{max} - a_{min})/a \leq 0.1 \tag{2}$$

$$\alpha = a/W \tag{3}$$

The fracture toughness K_{1C} was calculated as follows:

$$K_{IC} = \left[\frac{F_{max} \times S_0 \times 10^{-6}}{B \times W^{3/2}}\right]\left[\frac{3 \times (a/W)^{3/2}}{2 \times (1 - a/W)^{3/2}}\right] \cdot Y \tag{4}$$

where F_{max} is the maximum applied load at fracture, S_0 is the span of three-point bending, B is the sample width, and W is the sample thickness; Y is the dimensionless shape factor for average V-notch depth to the thickness of the sample W ratio [5]:

$$Y = \frac{1.99 - (a/W) \times (1 - a/W) \times [2.15 - 3.93 \times (a/W) + 2.7 \times (a/W)^2]}{1 + 2 \times (a/W)} \tag{5}$$

3. Results and Discussion

3.1. Displace-Loading Curves

The displacement-load curves of each test group are shown in Figure 5, and the repeatability of the tests was good. The fracture critical load of C-plane sapphire was significantly higher than that of other test groups. While the displacement of C-plane sapphire before fracture was also larger than that of the other test groups. The difference between the M-plane and A-plane sapphire was not obvious, the average value of fracture critical load was about 28 N and the average displacement with peak load was about 0.008 mm.

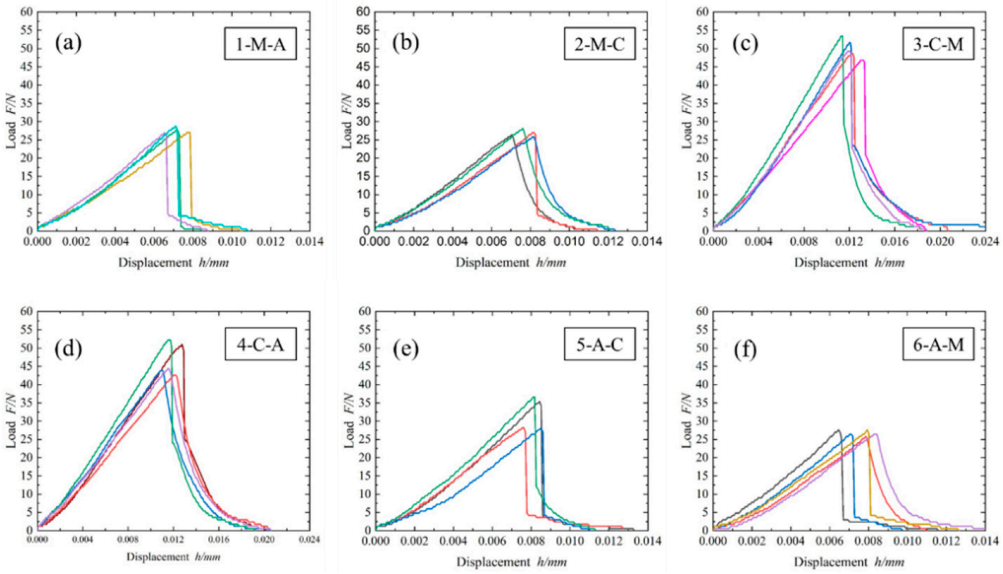

Figure 5. Displacement-load curves of each test group. (**a**) Test 1-M-A; (**b**) Test 2-M-C; (**c**) Test 3-C-M; (**d**) Test 4-C-A; (**e**) Test 5-A-C; (**f**) Test 6-A-M.

3.2. Calculation of K_{1C}

The results calculated according to Formulas (4) and (5) are shown in Table 4.

Table 4. Fracture toughness K_{1C} of each test group. (Unit: MPa·m$^{1/2}$).

Test Groups	K_{1C}-1	K_{1C}-2	K_{1C}-3	K_{1C}-4	K_{1C}-5	K_{1C}-6	K_{1C}-7	Average K_{1C}	
1-M-A	2.39	2.03	2.35	2.22	2.21	2.19	2.36	2.25	2.42
2-M-C	2.47	2.60	2.56	2.67	3.10 *	2.70	2.51	2.59	
3-C-M	4.04	4.26	4.45	4.44 *	4.27	4.13	4.12	4.21	4.24
4-C-A	4.37	4.36	4.28	2.53 *	4.30	3.95	4.36	4.27	
5-A-C	2.39	2.51	2.37	2.58 *	2.47 *	2.41	2.24	2.38	2.32
6-A-M	2.28	2.17	2.19	2.34	2.23	2.62 *	2.32	2.26	

Where the results marked * were not satisfied with Formula (2), and shall be removed. The experimental fracture toughness was consistent with the previous studies.

The comparison of fracture toughness calculation results of sapphire with different crystal orientations is shown in Figure 6. The fracture toughness of C-plane sapphire was about 4.24 MPa·m$^{1/2}$, and that of the other sapphires were close, with an average of 2.37 MPa·m$^{1/2}$. The fracture toughness of C-plane sapphire was significantly higher than others, about 77%. In tests with M-plane sapphire, the fracture toughness of pressuring C-plane was about 0.34 MPa·m$^{1/2}$ higher than that of pressuring A-plane. In tests with A-plane sapphire, the fracture toughness of pressuring the C-plane was close to that of pressuring M-plane. In general, the experimental fracture toughness of different crystal planes decreases in the order of C-plane > M-plane > A-plane.

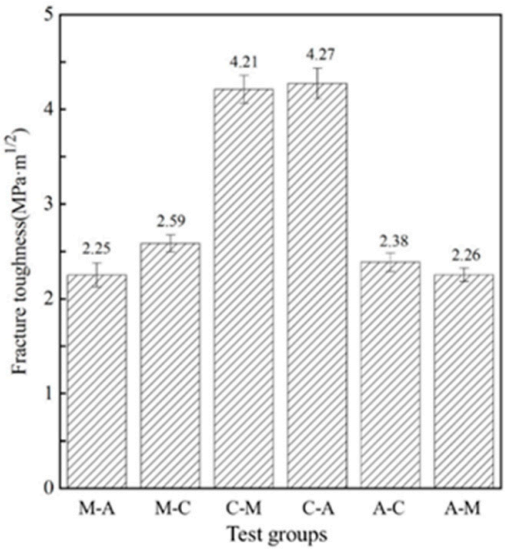

Figure 6. The average fracture toughness of each group.

As a result, from the displacement-load curves and fracture toughness K_{1C}, the fracture resistance of C-plane sapphire was much greater than that of sapphire with other orientations. Different crystal orientations showed anisotropy, and this was related to the loading plane.

3.3. Morphology of the Fractured Surface

The results of the compressive fracture of three different sapphire samples are shown in Figure 7. The test results of the same type of sapphire have relatively consistent surface morphology. Assuming that the sapphire samples tested have a perfect crystal structure, this paper makes the following analysis.

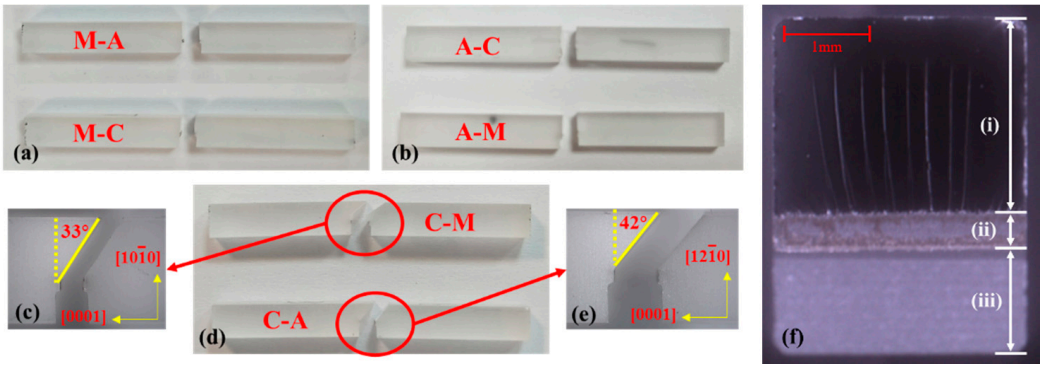

Figure 7. Fractured specimens. (**a**) Fracture of M-plane sapphire, where "M" is the cross-section of the sapphire sample, "A" and "C" are the loaded surfaces of the sapphire sample. (**b**) Fracture of A-plane sapphire, where "A" is the cross-section of the sapphire sample, "C" and "M" are the loaded surfaces of the sapphire sample. (**c**) Fracture of C-plane sapphire when loading M-plane. (**d**) Fracture of C-plane sapphire, where "C" is the cross-section of the sapphire sample, "M" and "A" are the loaded surfaces of the sapphire sample. (**e**) Fracture of C-plane sapphire when loading A-plane. (**f**) Fracture morphology with (i)-fracture zone, (ii)-V-notch zone, (iii)-U-notch groove zone.

The cleavage direction of M-plane and A-plane sapphires are parallel to the cross-section. It is obvious that the cleavage direction of C-plane sapphire is deflected, it is not along the cross-section of the sample. In addition, the fracture toughness of C-plane sapphire is the highest. According to the crystal structure of sapphire and the bond strength between different atoms, the results of experience are consistent with the expectation. In the C-plane sapphire tests, the angle between the cleavage direction and the cross-section (C-

plane) is 33 degrees when the M-plane is used as the loading surface. When the A-plane is used as the loading surface, the angle between the cleavage direction and the cross-section (C-plane) is 42 degrees. Theoretically, along the c-direction, there are only interchanging O–Al layers and hence cleavage is not favored. On the other hand, along the r-direction, weaker O–O layers are present and so cleavage is favored [27]. In fact, measurements of the fracture surface energy previously performed by Wiederhorn et al. [34], using the double-cantilever technique, showed that a crack propagating along the C-plane requires over six times more energy than along the R-plane. In the tests of C-plane sapphire, the pre-crack was on the C-plane, and it was predicted that the crack would propagate along the R-plane and cleavage would occur. If the cleavage along the R-plane occurs when the M-plane is used as the loading surface, the fracture surface forms 32.4 degrees with the m-direction. When the A-plane is the loading surface, the angle between the fracture surface and a-direction is 47 degrees. The experimental results are very close to the results of the crystallographic analysis, so it can be considered that the cleavage plane of C-plane sapphire is R-plane. This result is consistent with a study by Graça et al., and previous research [26]. Besides, the results of the M-plane and A-plane sapphire are similar, and cleavage was along the cross-section.

The morphology of the fractured surface was studied by a scanning electron microscope and three-dimensional video microscopy, as shown in Figure 7f. The fracture surface cracks of single-crystal sapphire with different crystal orientations also showed obvious anisotropy, with different degrees of crack propagation and surface fracture.

In the M-plane sapphire tests, when the A-plane was used as the loading surface, the cracks propagated vertically along *a*-direction, and then cleavage with long cracks. The cracks were large and very obvious, as shown in Figure 8a. At both sides of the section, the main cracks were about 30 degrees with *a*-direction. In addition, along the long cracks, there were many small transverse steps, as shown in Figure 8b. Swain et al. have explained this cleavage step deformation in brittle solids. Their occurrence could be satisfactorily explained in terms of a deflection in the base fracture of the near-symmetrical connecting sliver from one end to the other. Such a deflection would require only a small disturbance in stress conditions at the advancing crack front [35].

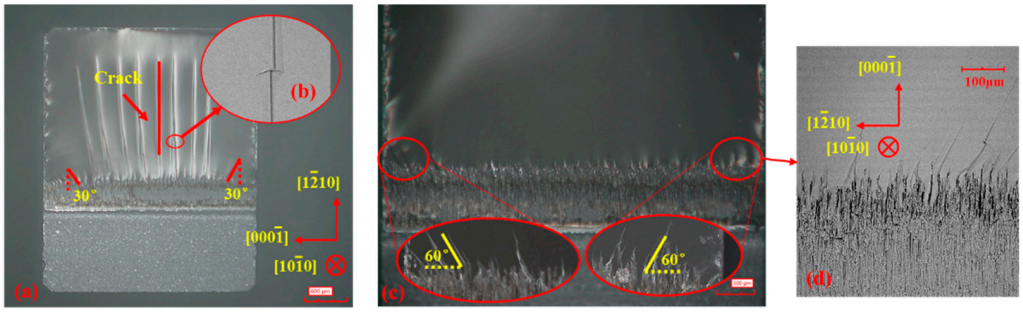

Figure 8. Morphology of the fractured surface in M-plane sapphire tests. (**a**) Fractured surface of M-A tests, "M" is the cross-section of the sapphire sample, "A" is the loaded surfaces. (**b**) Small transverse steps along cracks. (**c**) Fractured surface of M-C tests, "M" is the cross-section of the sapphire sample, "C" is the loaded surfaces. (**d**) Local cracks.

When the C-plane was used as the loading surface, cleavage was along the *c*-direction. The fractured surface was smooth and flat with short pre-crack propagation, as shown in Figure 8c. The crack propagation in the middle of the section was along the *c*-direction. At both sides of the section, the main cracks were about 60 degrees with *a*-direction, as shown in Figure 8d.

In C-plane sapphire tests, when the M-plane was used as the loading surface, initially, there were thick and short triangular cracks along the *m*-direction, and when the cracks disappeared, the section became smooth and flat, as shown in Figure 9a,b. Earlier, it can be confirmed that the cleavage of C-plane sapphire is along the R-plane in Figure 7d. Due

to the crystal structure being symmetrical along the *m*-direction in C-plane sapphire, the trend of crack propagation along the *r*-direction is counteracted. So, the length of the initial cracks was short, and the section was smooth and flat. When the A-plane was used as the loading surface, the whole fracture surface showed inclined long and thin cracks, as shown in Figure 9c,d. Cracks were formed at an angle of 57 degrees with *m*-direction. It was very close to the angle of 57.6 degrees between the M-plane and *r*-direction from the crystal structure. It also confirmed that the cleavage of the C-plane sapphire is along the R-plane; however, due to the crystal structure was not symmetrical along the *a*-direction, and CR-cracks were formed.

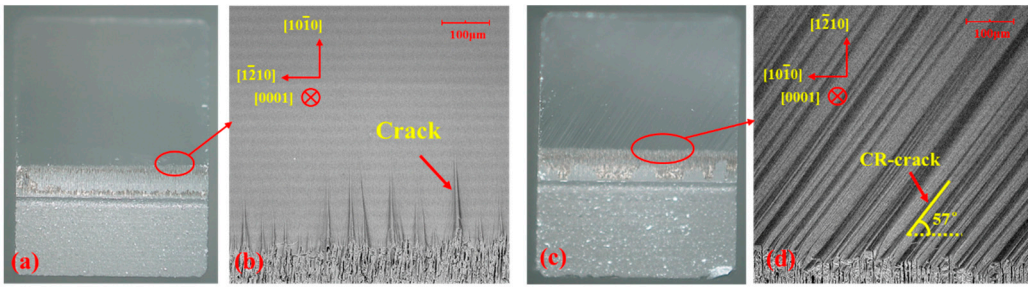

Figure 9. Morphology of the fractured surface in C-plane sapphire tests. (**a**) Fractured surface of C-M tests, "C" is the cross-section of the sapphire sample, "M" is the loaded surfaces. (**b**) Local cracks. (**c**) Fractured surface of C-A tests, "C" is the cross-section of the sapphire sample, "A" is the loaded surfaces. (**d**) Local cracks.

In the A-plane sapphire tests, the fracture direction was parallel to the section. No matter loading C-plane or M-plane, the section was smooth without crack, as shown in Figure 10a,c. It is considered that the cleavage direction is along the A-plane. Cleavage is along the *c*-direction when loading the C-plane, as shown in Figure 10b. On the other hand, cleavage is along the *m*-direction when loading the M-plane, as shown in Figure 10d.

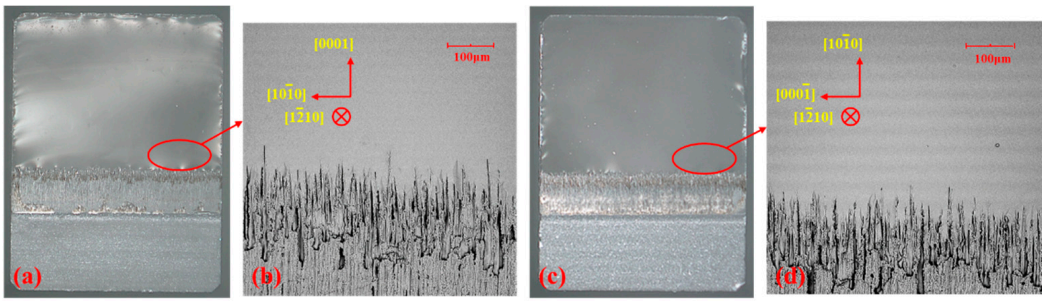

Figure 10. Morphology of the fractured surface in A-plane sapphire tests. (**a**) Fractured surface of A-C tests, "A" is the cross-section of the sapphire sample, "C" is the loaded surfaces. (**b**) Local cracks. (**c**) Fractured surface of A-M tests, "A" is the cross-section of the sapphire sample, "M" is the loaded surfaces. (**d**) Local cracks.

The fracture characteristics of the specimens are summarized in Table 5. The M-plane sapphire and A-plane sapphire are cleaved along the cross-section, which showed lower fracture toughness. The cleavage of C-plane sapphire is along the R-plane, and it showed the highest fracture toughness.

Table 5. Summary of the fracture characteristics of the specimens.

Sample	Loaded Surface	Cleavage Direction	Morphology of the Fractured Surface
M-Plane sapphire	A-plane	*a*-direction	Long large cracks with small transverse steps
M-Plane sapphire	C-plane	*c*-direction	Flat and smooth with short crack growth
C-Plane sapphire	M-plane	*r*-direction	Flat with thick and short triangular cracks
C-Plane sapphire	A-plane	*r*-direction	Very rough surface with 57° cracks
A-Plane sapphire	C-plane	*c*-direction	Flat and smooth without cracks
A-Plane sapphire	M-plane	*m*-direction	Flat and smooth without cracks

In addition, the formation and propagation of cracks must also be considered. Low-mobility dislocations, impurities, grain boundaries, and residual stresses are potential factors for crack nucleation and propagation. The high density and low mobility growth dislocations in the material lead to a decrease in fracture resistance. Due to not enough moving dislocations, the energy introduced cannot be dissipated by the classical plastic deformation mechanism, so it must be dissipated by fracture. In addition, impurities and crystal defects in the material lead to a decrease in fracture resistance. Besides, due to the grain boundary, crack propagation is restricted. For example, the grain boundary will lead to crack deflection to decrease the stress intensity at the crack tip, and the driving force of crack propagation is reduced [26]. The cracks formed and the propagation of single-crystal sapphire is complex, which needs further study in this paper.

3.4. Roughness of the Fractured Surface

The surface roughness of the fracture section was measured by the three-dimensional optical profiler. The measured results are shown in Figure 11. The single-crystal sapphire with different crystal orientations still showed obvious anisotropic. The roughness of different crystal planes decreased in the order of C-plane > M-plane > A-plane, the same as the order of fracture toughness. Roughness affects the dissipation of fracture energy and fracture toughness, the rougher the fracture surface is, the higher the fracture toughness is.

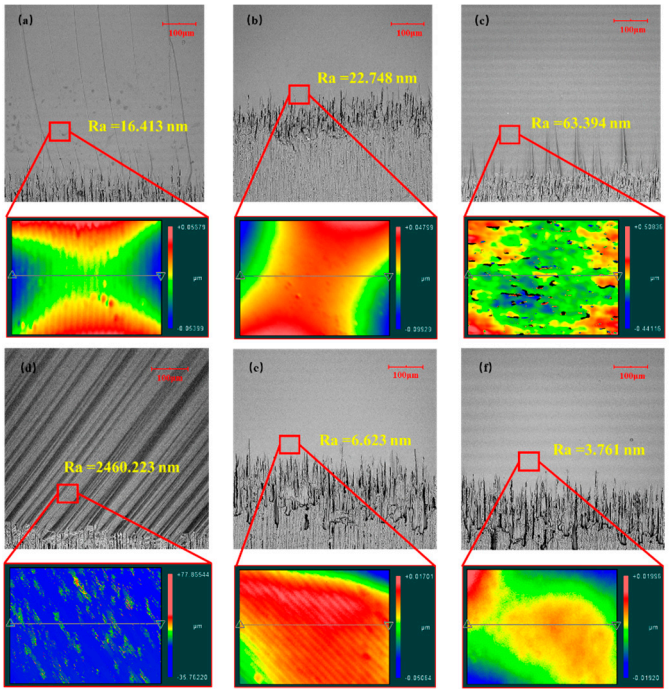

Figure 11. The roughness of the fracture section. (**a**) Test 1-M-A; (**b**) Test 2-M-C; (**c**) Test 3-C-M; (**d**) Test 4-C-A; (**e**) Test 5-A-C; (**f**) Test 6-A-M.

The fracture surfaces of "1-M-A", "2-M-C", "5-A-C", and "6-A-M" test groups were very smooth, because of the intergranular fracture [36]. Even though the fracture section of "1-M-A" test has many long cracks, other zones were also very smooth. Due to the inclined fracture of the C-plane sapphire, the fracture surface was very rough, and it showed a strong ability to resist fracture. With the obvious oblique cracks, the "4-C-A" test showed the largest surface roughness.

4. The Critical Resolved Shear Stress for Fracture Opening

Above this paper, the C-plane sapphire cleaves along the R-plane by crystallography analysis, and M-, A-plane sapphires cleave along their cross-section. Does sapphire undergo plastic deformation before dissociation fracture? Mizumoto et al. have conducted plunge-cut tests to deeply analyze the brittle-ductile transition on the basal (0001) plane. The anisotropic deformation behavior of sapphire is discussed in terms of slip system, cleavage, and twinning [37].

The tendency for plastic deformation can be expressed by the resolved shear stress on a specific slip system. Schmid's law describes the relationship between the resolved shear stress and slip system [38] by:

$$\tau = \sigma_a \cdot m \tag{6}$$

$$m = cos\varphi cos\lambda \tag{7}$$

where τ is the resolved shear stress, σ_a is the applied stress, m is the Schmid-factor, φ is the angle between the applied stress and slip plane, λ is the angle between the applied stress and slip direction, as shown in Figure 12. If the resolved shear stress surpasses the CRSS, the slip system will be activated. The Schmid-factor m quantifies how easily the slip system is activated, and so is the twinning system. The CRSS value in possible slip and twin systems of single-crystal sapphire is shown in Table 1.

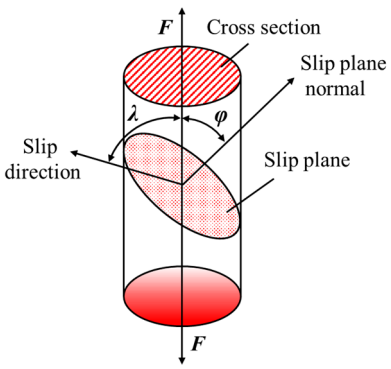

Figure 12. Slip deformation of a single-crystal specimen under uniaxial tension.

In this study, we have obtained K_{1C} of single-crystal sapphire with different orientations, as seen in Table 4. The applied stress can be calculated by:

$$\sigma_a = \frac{K_{1C}}{\sqrt{\pi r}} \tag{8}$$

where r is the cutting depth of laser about 0.5 mm.

The resolved shear stress was calculated by Formulas (6)–(8). The result was showed in Table 6.

Table 6. Calculation of the resolved shear stress [28].

Sample	K_{1C} (MPa·m$^{1/2}$)	r (mm)	σ_a (MPa)	Plastic Deformation	*CRSS* (GPa)	φ (°)	λ (°)	m	τ (GPa)	Activation
					Slip/Twin					Slip/Twin
M-plane sapphire	2.42	0.5	193	Rhombohedral plane	3/0.111	57.6	32.4	0.45	0.087	N/N
				Basal plane	17/0.148	0	90	0	0	N/N
				Prism plane	1.2/-	90	0	0	0	N/-
C-plane sapphire	4.24	0.5	338	Rhombohedral plane	3/0.111	32.4	57.6	0.45	0.152	N/Y
				Basal plane	17/0.148	90	0	0	0	N/N
				Prism plane	1.2/-	0	90	0	0	N/-
A-plane sapphire	2.32	0.5	185	Rhombohedral plane	3/0.111	57.6	32.4	0.45	0.083	N/N
				Basal plane	17/0.148	0	90	0	0	N/N
				Prism plane	1.2/-	90	0	0	0	N/-

Where "N" means that plastic deformation is not activated, "Y" means that plastic deformation is activated.

Only in C-plane sapphire tests, cleavage is along the R-plane with 57.6 degrees. The resolved shear stress (0.152 GPa) surpasses the CRSS (0.111 GPa), so the rhombohedral twin is activated probably before dissociation fracture. In other sample tests, the resolved shear stress did not surpass the CRSS of plastic deformation, and the plastic degeneration would not be activated before dissociation fracture.

5. Conclusions

(1) The fracture toughness of single-crystal sapphire with different crystal planes showed anisotropy. The fracture toughness of C-plane sapphire was highest than other orientations. Fracture toughness of different crystal planes decreases in the order of C-plane > M-plane > A-plane.

(2) The fracture morphology of single-crystal sapphire with different crystal faces shows obvious anisotropy, different cracks growth, and morphology. In M-plane sapphire, there are many long cracks on the fracture when loading A-plane. In C-plane sapphire, the whole fracture presents inclined cracks with 57 degrees when loading A-plane. The fracture surfaces of other samples are smooth. The roughness of different crystal planes decreased in the order of C-plane > M-plane > A-plane, the same as the order of fracture toughness. The surface roughness will affect the dissipation of fracture energy. With a larger the fracture toughness value, the ability of sapphire to resist fracture is stronger.

(3) C-plane sapphire cleavages along the R-plane with an angle of 57.6 degrees. M-plane and A-plane sapphire cleavages along their cross-section. The cleavage fracture of C-plane sapphire seems to be related to the rhombohedral twin. The rhombohedral twin promotes crack propagation and forms the fracture morphology of inclined cracks.

Author Contributions: Conceptualization, F.J. and S.H.; methodology, J.L.; validation, X.L., F.J. and Q.W.; formal analysis, S.H.; investigation, B.G.; resources, N.W.; data curation, S.H.; writing—original draft preparation, S.H.; writing—review and editing, F.J.; visualization, B.G.; supervision, Q.W.; project administration, F.J. All authors have read and agreed to the published version of the manuscript.

Funding: This research was funded by the National Natural Science Foundation of China (No. 51805176) and the Natural Science Foundation of Fujian (Grant No. 2019J01059).

Data Availability Statement: Data can be obtained by contacting the corresponding author.

Conflicts of Interest: The authors declare no conflict of interest. The funders had no role in the design of the study.

References

1. Salem, J.A.; Quinn, G.D. Fractographic analysis of large single crystal sapphire refractive secondary concentrators. *J. Eur. Ceram. Soc.* **2014**, *34*, 3271–3281. [CrossRef]

2. Khattak, C.P.; Shetty, R.; Schwerdtfeger, C.R.; Ullal, S. World's largest sapphire for many applications. *J. Cryst. Growth* **2016**, *452*, 44–48. [CrossRef]
3. Huang, H.; Li, X.; Mu, D.; Lawn, B.R. Science and art of ductile grinding of brittle solids. *Int. J. Mach. Tools Manuf.* **2020**, *161*, 103675. [CrossRef]
4. Bao, Y.; Zhou, Y. A new method for precracking beam for fracture toughness experiments. *J. Am. Ceram. Soc.* **2006**, *89*, 1118–1121. [CrossRef]
5. Sakai, M.; Bradt, R.C. Fracture toughness testing of brittle materials. *Int. Mater. Rev.* **1993**, *38*, 53–78. [CrossRef]
6. Wan, D.; Wei, Y.; Bao, Y.; Tian, Y. Comparison and Analysis of the Accuracy and Convenience of Ceramic Fracture Toughness Testing Methods. *J. Chin. Ceram. Soc.* **2019**, *47*, 1080–1088.
7. Zhao, W.; Rao, P.; Ling, Z. A new method for the preparation of ultra-sharp V-notches to measure fracture toughness in ceramics. *J. Eur. Ceram. Soc.* **2014**, *34*, 4059–4062. [CrossRef]
8. Quinn, G.D.; Swab, J.J. Fracture toughness of glasses as measured by the SCF and SEPB methods. *J. Eur. Ceram. Soc.* **2017**, *37*, 4243–4257. [CrossRef]
9. Yanaba, Y.; Hayashi, K. Relation between fracture surface area of a flexural strength specimen and fracture toughness for WC-10mass% Co cemented carbide and Si3N4 ceramics. *Mater. Sci. Eng. A* **1996**, *209*, 169–174. [CrossRef]
10. Zhao, Q.; Wang, Y.; Yu, G.; Dong, S.; Zhang, X. Investigation of anisotropic mechanisms in ultra-precision diamond machining of KDP crystal. *J. Mater. Process. Technol.* **2009**, *209*, 4169–4177. [CrossRef]
11. Wen, Q.; Wei, X.; Jiang, F.; Lu, J.; Xu, X. Focused Ion Beam Milling of Single-Crystal Sapphire with A-, C-, and M-Orientations. *Materials* **2020**, *13*, 2871. [CrossRef] [PubMed]
12. Wen, Q.; Zhang, P.; Cheng, G.; Jiang, F.; Lu, X. Crystalline orientation effects on material removal of sapphire by femtosecond laser irradiation. *Ceram. Int.* **2019**, *45*, 23501–23508. [CrossRef]
13. Wang, L.; Hu, Z.; Chen, Y.; Yu, Y.; Xu, X. Material removal mechanism of sapphire substrates with four crystal orientations by double-sided planetary grinding. *Ceram. Int.* **2020**, *46*, 7813–7822. [CrossRef]
14. Luo, Q.; Lu, J.; Xu, X.; Jiang, F. Removal mechanism of sapphire substrates (0001, 11-20 and 10-10) in mechanical planarization machining. *Ceram. Int.* **2017**, *43*, 16178–16184. [CrossRef]
15. Wang, N.; Jiang, F.; Xu, X.; Duan, N.; Wen, Q.; Lu, X. Research on the machinability of A-plane sapphire under diamond wire sawing in different sawing directions. *Ceram. Int.* **2019**, *45*, 10310–10320. [CrossRef]
16. Luan, X.; Jiang, F.; Wang, N.; Xu, X.; Lu, X.; Wen, Q. The mechanical response characteristics of sapphire under dynamic and quasi-static indentation loading. *Ceram. Int.* **2018**, *44*, 15208–15218. [CrossRef]
17. Jiang, F.; Luan, X.; Wang, N.; Xu, X.; Lu, X.; Wen, Q. Research on the dynamic mechanical properties of C-plane sapphire under impact loading. *Ceram. Int.* **2018**, *44*, 9839–9847. [CrossRef]
18. Wang, N.; Jiang, F.; Xu, X.; Lu, X. Effects of crystal orientation on the crack propagation of sapphire by sequential indentation testing. *Crystals* **2018**, *8*, 3. [CrossRef]
19. Wang, K.; Jiang, F.; Yan, L.; Xu, X.; Wang, N.; Zha, X.; Lu, X.; Wen, Q. Study on mechanism of crack propagation of sapphire single crystals of four different orientations under impact load and static load. *Ceram. Int.* **2019**, *45*, 7359–7375. [CrossRef]
20. Wan, L.; Dai, P.; Li, L.; Deng, Z.; Hu, Y. Investigation on ultra-precision lapping of A-plane and C-plane sapphires. *Ceram. Int.* **2019**, *45*, 12106–12112. [CrossRef]
21. Wang, K.; Jiang, F.; Li, Y.; Wang, N.; Hu, Z.; Yan, L.; Lu, J.; Wen, Q.; Lu, X. Prediction of pop-in load for sapphires with different crystal orientations. *Ceram. Int.* **2020**, *46*, 6682–6692. [CrossRef]
22. Lin, J.; Jiang, F.; Xu, X.; Lu, J.; Tian, Z.; Wen, Q.; Lu, X. Molecular dynamics simulation of nanoindentation on c-plane sapphire. *Mech. Mater.* **2021**, *154*, 103716. [CrossRef]
23. Lin, J.; Jiang, F.; Wen, Q.; Wu, Y.; Lu, J.; Tian, Z.; Wang, N. Deformation anisotropy of nano-scratching on C-plane of sapphire: A molecular dynamics study and experiment. *Appl. Surf. Sci.* **2021**, *546*, 149091. [CrossRef]
24. Azhdari, A.; Nemat-Nasser, S.; Rome, J. Experimental observations and computational modeling of fracturing in an anisotropic brittle crystal (sapphire). *Int. J. Fract.* **1998**, *94*, 251–266. [CrossRef]
25. Konstantiniuk, F.; Tkadletz, M.; Kainz, C.; Czettl, C.; Schalk, N. Mechanical properties of single and polycrystalline α-Al2O3 coatings grown by chemical vapor deposition. *Surf. Coat. Technol.* **2021**, *410*, 126959. [CrossRef]
26. Graça, S.; Trabadelo, V.; Neels, A.; Kuebler, J.; Le Nader, V.; Gamez, G.; Döbeli, M.; Wasmer, K. Influence of mosaicity on the fracture behavior of sapphire. *Acta Mater.* **2014**, *67*, 67–80. [CrossRef]
27. Dobrovinskaya, E.R.; Lytvynov, L.A.; Pishchik, V. *Sapphire: Material, Manufacturing, Applications*; Springer: New York, NY, USA, 2009.
28. Nowak, R.; Sakai, M. The Anisotropy of Surface Deformation of Sapphire: Continuous Indentation of Triangular Indenter. *Acta Metall. Et Mater.* **1994**, *42*, 2879–2891. [CrossRef]
29. Guan, Z.; Zhang, Z.; Jiao, J. *Physical Properties of Inorganic Materials*; Tsinghua University Press: Beijing, China, 2004.
30. Nose, T.; FUJII, T. Evaluation of fracture toughness for ceramic materials by a single-edge-precracked-beam method. *J. Am. Ceram. Soc.* **1988**, *71*, 328–333. [CrossRef]
31. Dukino, R.D.; Swain, M.V. Comparative measurement of indentation fracture toughness with Berkovich and Vickers indenters. *J. Am. Ceram. Soc.* **1992**, *75*, 3299–3304. [CrossRef]
32. Fischer, H.; Waindich, A.; Telle, R. Influence of preparation of ceramic SEVNB specimens on fracture toughness testing results. *Dent. Mater.* **2008**, *24*, 618–622. [CrossRef] [PubMed]

33. *ISO 23146: Fine Ceramics (Advanced Ceramics, Advanced Technical Ceramics)—Test Method for Fracture Toughness of Monolithic Ceramics-Single-Edge V-Notch Beam (SEVNB) Method*; ISO: Geneva, Switzerland, 2012.
34. Wiederhorn, S.M.; Hockey, B.J.; Roberts, D.E. Effect of temperature on the fracture of sapphire. *Philos. Mag. A J. Theor. Exp. Appl. Phys.* **1973**, *28*, 783–796. [CrossRef]
35. Swain, M.V.; Lawn, B.R.; Burns, S.J. Cleavage step deformation in brittle solids. *J. Mater. Sci.* **1974**, *9*, 175–183. [CrossRef]
36. Zhang, T.; Jiang, F.; Huang, H.; Lu, J.; Xu, X. Towards understanding the brittle-ductile transition in the extreme manufacturing. *Int. J. Extrem. Manuf.* **2021**, *3*, 022001. [CrossRef]
37. Mizumoto, Y.; Maas, P.; Kakinuma, Y.; Min, S. Investigation of the cutting mechanisms and the anisotropic ductility of monocrystalline sapphire. *CIRP Ann.—Manuf. Technol.* **2017**, *66*, 89–92. [CrossRef]
38. Schmid, E.; Boas, W. *Plasticity of Crystals*; FA Hughes & Co, Ltd.: London, UK, 1950.